Asian Journal of Chemistry; Vol. 37, No. 6 (2025), 1509-1517

ASIAN JOURNAL OF CHEMISTRY

https://doi.org/10.14233/ajchem.2025.33500

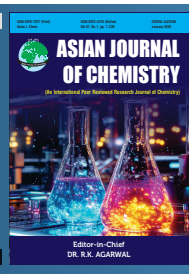

Synthesis, Structural Characterization and Anticancer Evaluation of 2-Aminobenzothiazole Derivative *via* Benzoyl Isothiocyanate

SIDDHIMA SHARMA[1,*], LALIMA SHARMA[1], RENU RATHORE[2], D. VIJAY[3] and MANGAL SHREE DULAWAT[1]

[1]Department of Chemistry, J.R.N. Rajasthan Vidyapeeth (Deemed to be University), Udaipur-313001, India
[2]Department of Chemistry, Faculty of Science, Bhupal Nobles' University, Udaipur-313001, India
[3]Department of Physics, D.N.R College (A), Bhimavaram-534202, India

*Corresponding author: E-mail: siddhimasharma18@gmail.com

Received: 12 February 2025; *Accepted*: 24 May 2025; *Published online*: 27 May 2025; AJC-22025

2-Aminobenzothiazole derivatives are well-established scaffolds in medicinal chemistry, valued for their diverse pharmacological profiles. In this study, a novel synthetic route led to the development of *N*-(1,3-benzothiazol-2-yl)benzamide (SIBO), whose structure was thoroughly characterized *via* FTIR, NMR, HRMS and SC-XRD techniques. The experimentally determined crystal geometry was further supported by DFT calculations at the B3LYP/6-31G(d,p) level, showing excellent agreement in bond parameters and a moderate HOMO–LUMO energy gap indicative of potential bioactivity. Hirshfeld surface analysis highlighted key intermolecular interactions contributing to the stability of the crystal lattice. Preliminary *in vitro* cytostatic screening against MDA-MB-231 and MCF-7 breast cancer cell lines revealed dose-dependent growth inhibition, with SIBO reducing MDA-MB-231 cell viability by up to 52% at 10 µg/mL. Although its efficacy was lower to that of standard adriamycin, the selective activity and structural simplicity of SIBO indicate its potential as a lead compound for the development of safer and tailored anticancer drugs.

Keywords: 2-Aminobenzothiazole, DFT calculations, Hirshfeld surface analysis, Breast cancer cell lines, Anticancer activity.

INTRODUCTION

2-Aminobenzothiazoles are a significant class of nitrogen and sulfur containing heterocycles, widely recognized for their diverse pharmacological properties such as notable for their diverse therapeutic potential, including activity against bacterial infections, cancer, inflammation and viral diseases [1,2]. Due to their broad biological relevance, these compounds frequently appear as core structures in various bioactive compounds used in medicine and agricultural applications, positioning them as key targets in medicinal and synthetic organic chemistry [3,4]. Conventionally, their synthesis relies on the oxidative cyclization of 2-aminothiophenols with nitriles, thiourea derivatives, or other sulfur-donating precursors [5-7]. Among the various synthetic strategies developed to date, the use of isothiocyanate derivatives has drawn growing interest owing to their ability to undergo efficient cyclization with nucleophilic substrates [8-11]. Aromatic isothiocyanates, in particular, provide structural versatility and have been explored for constructing sulfur and nitrogen-based heterocyclic systems [12].

In this context, 2-haloanilines serve as excellent nucleophilic partners due to the activating effect of the *ortho*-halogen, which promotes intramolecular cyclization by enhancing the electrophilicity of the adjacent carbon atom [13-15]. Their synthetic utility is further amplified by the halogen's role as a reactive handle for post-synthetic modifications through cross-coupling reactions. On the electrophilic counterpart, benzoyl isothiocyanate (BOITC), though less common in nature, offers a distinct and underutilized alternative to conventional isothiocyanates. BOITC has been synthesized and studied primarily for its reactivity in the formation of thiourea and heterocyclic frameworks. Biological investigations on BOITC emerging reports have highlighted its antimicrobial, cytotoxic and anti-inflammatory potential [16-20]. The presence of the electron-withdrawing benzoyl group in BOITC significantly alters its reactivity profile, making it a unique electrophile for heterocyclic synthesis.

Despite these promising features, the use of BOITC, as core building blocks in the synthesis of N–S heterocycles remain

relatively underexplored. In the present study, we report a synthetic route for 2-aminobenzothiazole derivative *N*-(1,3-benzothiazol-2-yl)benzamide utilizing benzoyl isothiocyanate and 2-haloanilines using CuBr as catalyst, Cs_2CO_3 as base and glycine as ligand to facilitate efficient synthesis under mild conditions. Although N-(1,3-benzothiazol-2-yl) benzamide is a known compound, the current study presents a novel, direct, one-pot synthetic route that streamlines the synthesis and improves overall efficiency. The molecular structure was confirmed using a combination of NMR, IR, mass spectrometry and SCXRD, were employed to confirm the structure of the synthesized compound. In addition to the standard characterization methods, the crystal data were utilized to analyze intermolecular interactions in detail. Hydrogen bonding contacts, van der Waals interactions and Hirshfeld surface analysis were performed to gain deeper insights into the molecular packing and interaction patterns, aspects which have not been previously explored for this compound. Moreover, DFT calculations were carried out and the theoretical data were systematically compared with experimental results to validate the molecular geometry and electronic features. The anticancer efficacy was assessed using MDA-MB-231 and MCF-7 breast carcinoma cell lines using the sulforhodamine B (SRB) assay. The results demonstrated promising cytotoxic effects, indicating the compound's potential as a lead candidate for breast cancer therapy.

EXPERIMENTAL

N-(1,3-benzothiazol-2-yl)benzamide (SIBO) compound was synthesized using reagents sourced from Sigma-Aldrich. Reaction progress was monitored by thin-layer chromatography (TLC) on silica gel plates with an aluminium backing. Spots were visualized under ultraviolet light at a wavelength of 254 nm. The melting point of the compound was measured using a microprocessor melting point apparatus (model S-972). FTIR analysis was performed with a Perkin-Elmer spectrum 2 spectrometer to identify the functional groups. Proton (^{1}H) and carbon (^{13}C) NMR spectra were recorded on a Bruker Avance Neo 500 MHz spectrometer to confirm the structural details. HRMS was conducted using a Waters Synapt XS HDMS instrument to determine the accurate molecular mass.

Synthesis process: A solution of benzoyl isothiocyanate (0.70 mmol) in DMF (2.4 mL) was added dropwise to a stirred mixture of 2-iodoaniline or 2-bromoaniline (0.60 mmol), cesium carbonate (1.2 mmol), copper(I) bromide (0.07 mmol, 10 mol%) and glycine (0.13 mmol, 20 mol%) in DMF (2.0 mL). The reaction mixture was refluxed for 2 h. Reaction progress was monitored by TLC using ethyl acetate/hexane (1:1) as eluent. After completion of the reaction, the mixture was cooled to ambient temperature and the solvent was evaporated under reduced pressure. The crude residue was then subjected to column chromatography to isolate the compound in good yield (**Scheme-I**). Dark yellow, yield: 82%, m.p.: 198 ºC; IR (KBr, ν_{max}, cm^{-1}): 3426 (O–H), 3239 (N–H *str.*), 2071 (C≡N *str.*), 1662 (C=O *str.*), 1599 (C=C arom. *str.*),1279 (C–N *str.*); ^{1}H NMR (DMSO,500 MHz, δ ppm): 12.88 (s, 1H), 8.14 (d, *J* = 8.2 Hz, 2H), 8.02 (d, *J* = 8.0 Hz, 1H), 7.80 (d, *J* = 8.0 Hz,1H), 7.67 (t, *J* = 7.7 Hz, 1H), 7.56 (t, *J* = 7.6 Hz, 2H), 7.47 (t, *J* = 7.5 Hz, 1H), 7.35 (t, *J* = 7.4 Hz, 1H); ^{13}C NMR (DMSO, 125 MHz, δ ppm): 165.9 (C8), 158.8 (C7), 148.2 (C6), 132.8 (C9), 131.8 (C10), 131.4 (C1),128.5 (C11, C13), 128.2 (C12, C14), 126.1 (C5), 123.6 (C3), 121.6 (C2), 120.2 (C4). HRMS (ES^+): *m/z* 255.05 (calcd. for $C_{14}H_{10}N_2OS$ $[M + H]^+$), 255.06 (found).

Crystal structure determination: Single crystals of the SIBO, transparent and needle-shaped, was carefully selected for X-ray diffraction analysis. Data collection was performed at room temperature (296.15 K) using a Bruker APEX-II CCD diffractometer. The initial crystal structure solution was achieved through direct methods utilizing the SHELXS-97 program and subsequent refinement against squared structure factors (F^2) was carried out with SHELXL-97 software [21]. Hydrogen atoms bonded to carbon were modeled riding on their parent atoms, while those attached to heteroatoms were located from the Fourier difference electron density maps and refined with isotropic displacement parameters. All other atoms were refined anisotropically to improve accuracy. The thermal ellipsoid plot (ORTEP diagram) was acquired using ORTEP-3, while molecular visualization and examination of weak non-covalent interactions were performed using MERCURY software [22,23]. The crystallographic information file (.cif) for the SIBO compound has been deposited at the Cambridge Crystallographic Data Centre with accession number CCDC 2452417.

Computational approach: The molecular geometry of the SIBO was optimized using density functional theory methods implemented in Gaussian 09 Revision D.01. The calculations utilized the B3LYP functional combined with the 631G basis set enhanced with polarization functions. Preparation of input files and visualization of results were conducted through GaussView version 6 [24,25]. This computational procedure enabled precise evaluation of bond lengths, bond angles and dihedral angles, providing a well-optimized structural model of the molecule.

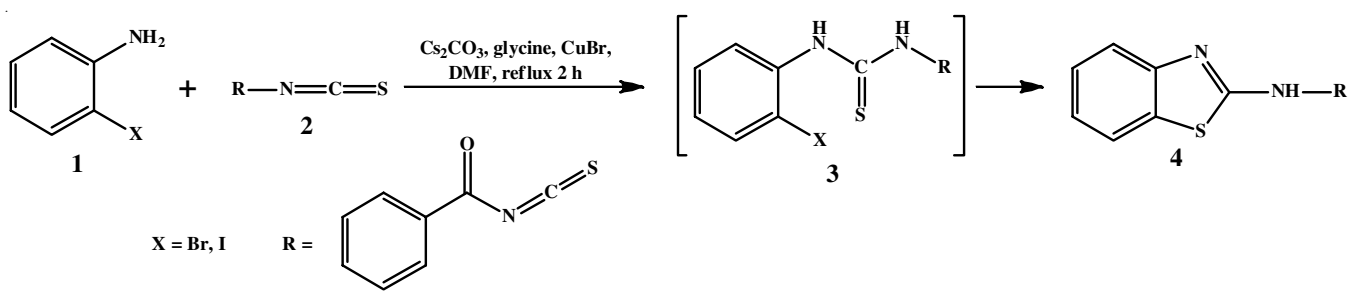

Scheme-I: Scheme for the synthesis of the title compound

Hirshfeld surface analysis: To investigate intermolecular forces and crystal packing patterns of the SIBO compound, Hirshfeld surface analysis was carried out using Crystal Explorer version 17.5. The refined crystallographic data of the compound was imported to generate the Hirshfeld surfaces along with 2D fingerprint plots [26]. The normalized contact distance maps were plotted over a range spanning from about, effectively illustrating regions where close intermolecular contacts occur within the crystal. The fingerprint plots offered a detailed quantitative representation of the various intermolecular interactions, shedding light on the packing efficiency and the nature of contacts within the crystal lattice.

Standard protocol for *in vitro* cytotoxicity testing using the sulforhodamine B (SRB) assay: Human breast cancer cell lines MDA-MB-231 (triple-negative) and MCF-7 (ER+, PR+) were cultured in DMEM and RPMI-1640 medium, respectively, each supplemented with 10% fetal bovine serum (FBS) and 2 mM L-glutamine. Cells were maintained at 37 ºC in a humidified atmosphere of 5% CO_2 and 95% air. For cytotoxicity screening, 5,000 cells/well were seeded into 96-well flat-bottom plates in 100 µL of complete growth medium. Plates were incubated for 24 h to allow cell attachment. Test compounds were initially dissolved in a suitable solvent (*i.e.* DMSO) at 100 mg/mL, then diluted to 1 mg/mL in distilled water and stored frozen. Before use, stock solutions were thawed and further diluted in complete medium to prepare working solutions of 100, 200, 400 and 800 µg/mL. From these, 10 µL was added to each well already containing 90 µL of medium, yielding final concentrations of 10, 20, 40 and 80 µg/mL.

Following drug treatment, cells were incubated under standard conditions for 48 h. The assay was then terminated by the addition of cold 30% trichloroacetic acid (TCA). To fix the cells, 50 µL of cold TCA was added to each well (final concentration: 10% TCA) and the plates were incubated at 4 ºC for 60 min. Supernatants were discarded and plates were rinsed five times with tap water and air dried. Each well was then stained with 50 µL of 0.4% sulforhodamine B (SRB) in 1% acetic acid and incubated at room temperature for 20 min. Unbound dye was removed by washing the plates five times with 1% acetic acid, followed by air drying. Protein-bound dye was solubilized using 10 mM Trizma base and absorbance was measured at 540 nm with a 690 nm reference wavelength.

Cell viability was calculated using the following formula:

$$\text{Growth (\%)} = \frac{\text{Average absorbance of treated wells}}{\text{Average absorbance of control wells}} \times 100$$

From absorbance values at time zero (T_0), control (C) and at each drug concentration (Ti), the percentage growth was determined. GI_{50}, the drug concentration resulting in 50% inhibition of net cell growth, was calculated for each cell line. If GI_{50} was not reached within the tested range, it was reported as greater than or less than the highest or lowest concentration tested.

RESULTS AND DISCUSSION

The synthesis of SIBO from 2-haloanilines and benzoyl isothiocyanate proceeds through an efficient tandem process, initiated by the formation of a thiourea intermediate, followed by copper(I) catalyzed intramolecular cyclization (**Scheme-I**). In the initial step, the nucleophilic amino group of aniline attacks the electrophilic carbon of isothiocyanate, yielding the corresponding thiourea intermediate. The substituent plays a crucial role in influencing the steric and electronic properties of the intermediate. For benzoyl isothiocyanate, the conjugated carbonyl group introduces increased electron-withdrawing character, potentially enhancing the acidity of thiourea NH and improving coordination with the copper catalyst, though the overall system is slightly more rigid. Under the reaction conditions, Cs_2CO_3 serves as a base, promoting deprotonation of thiourea and activation of the *ortho* C–H bond. Simultaneously, CuBr, in the presence of glycine, coordinates with the thiourea sulfur and activates the nearby aryl C–H bond *via* a metalation mechanism. This facilitates the formation of a five-membered benzothiazole ring through intramolecular C–S bond formation. The final step involves the elimination of a proton and re-aromatization, yielding the desired 2-aminobenzothiazole product.

The reaction is conducted in DMF, a polar aprotic solvent that effectively stabilizes both ionic and organometallic intermediates. The choice of DMF enhances the solubility of the reactants and catalytic species, contributing to the efficiency and consistency of the transformation. Overall, this tandem protocol provides a versatile and streamlined approach to constructing an aminobenzothiazole framework from benzoyl isothiocyanate substituents, under mild and operationally simple conditions.

Description of crystal structure: The single crystal of compound SIBO were successfully obtained using a slow evaporation technique from a mixed solvent system of DCM and EtOH. SC-XRD was employed to elucidate the solid-state structure of compound SIBO, with the empirical formula $C_{14}H_{10}N_2OS$ and a molecular weight of 254.30 g/mol (Fig. 1). A well-formed, colourless crystal with approximate dimensions of 0.28 mm × 0.24 mm × 0.21 mm was used for data collection at 296.15 K. The crystallographic analysis revealed that compound SIBO crystallizes in the monoclinic crystal system, adopting the centrosymmetric space group $P2_1/n$. The unit cell parameters were determined to be a = 5.9492(6) Å, b = 16.8592(17) Å, c = 11.9493(13) Å, with β = 102.484(3)º and right angles for α and γ. The unit cell volume was calculated as 1170.2(2) Å^3, containing four formula units (Z = 4).

The theoretical density of the crystal was calculated to be 1.443 g/cm^3 and the linear absorption coefficient (µ) for Mo$K\alpha$ radiation (λ = 0.71073 Å) was found to be 0.264 mm^{-1}. Data acquisition was performed over a 2θ range of 4.246º to 55.042º, yielding a total of 19,187 reflections, of which 2,698 were identified as independent (R_{int} = 0.0714; R_{sigma} = 0.0388). The structure was refined using full-matrix least-squares procedures on F^2, with 164 refined parameters and no restraints. The refinement yielded a goodness-of-fit value of 1.070.

The final R indices for observed reflections ($I \geq 2\sigma(I)$) were $R1$ = 0.0979 and $wR2$ = 0.2324, while the corresponding values for all data were $R1$ = 0.1340 and $wR2$ = 0.2814. The residual electron density map showed no significant anomalies, with the largest positive and negative peaks being +0.51 and –0.56 e Å^3, respectively. These results confirm the reliability and consistency of the obtained structural model.

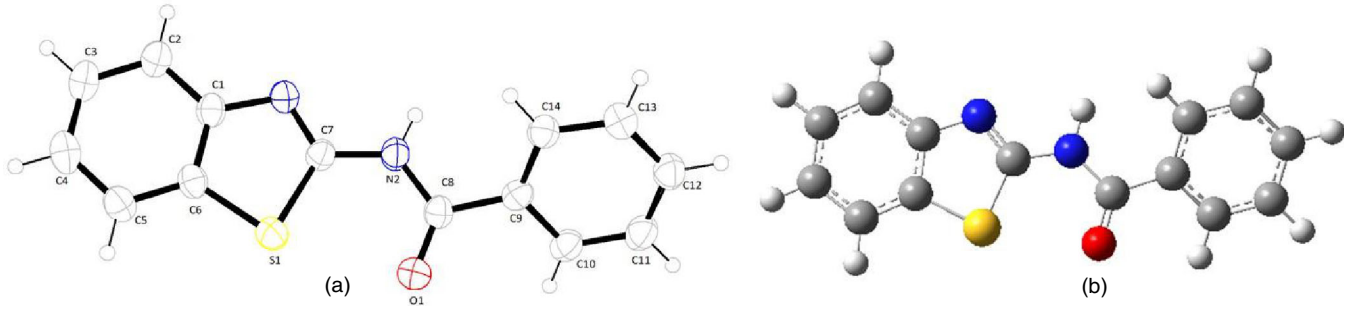

Fig. 1. (a) ORTEP diagram of the SIBO molecule drawn at 40% probability thermal ellipsoids, showing the atomic labeling scheme; (b) DFT-optimized molecular structure of SIBO illustrating the spatial arrangement of atoms

The crystal structure of SIBO reveals the presence of significant intermolecular hydrogen bonding interactions that contribute to the overall stabilization and organization of the molecular packing (Fig. 2a). A prominent feature is the bifurcated hydrogen bonding involving the N–H moiety (N1–H2), which simultaneously interacts with two distinct acceptor atoms. The first interaction occurs between the hydrogen atom H2 and a neighboring nitrogen atom (N1) from an adjacent molecule, forming a classical N–H···N hydrogen bond with a donor–acceptor distance of 2.254 Å. Simultaneously, the same hydrogen atom (H2) also engages in a second hydrogen bond with an oxygen atom (O1), yielding an N–H···O interaction with a comparable distance of 2.264 Å. This bifurcated arrangement suggests a cooperative interaction, enhancing the lattice stability through a three-centered hydrogen bonding motif. Moreover, a weaker yet structurally relevant C–H···O interaction is observed between the hydrogen atom H12 from a phenyl ring and the oxygen atom O1, with a donor–acceptor distance of 2.639 Å. Although C–H···O hydrogen bonds are typically considered weak, their presence in this system further supports the formation of a robust supramolecular framework.

The crystal structure of SIBO also exhibits a series of notable short contacts that further contribute to the molecular organization within the lattice (Fig. 2b). A distinct short contact is observed between the hydrogen atom H11 of the aromatic ring and the oxygen atom O8, with a contact distance of 2.866 Å, indicating a weak but meaningful C–H···O interaction. Another interaction involves H11 (from a neighbouring molecule) and the nitrogen atom N2A, forming a short contact at 2.865 Å, characteristic of a C–H···N type interaction. Furthermore, H10 is engaged in a C–H···N contact with N2A at a distance of 2.948 Å. These interactions are often overlooked due to their relative weakness compared to classical hydrogen bonds, yet in this structure, they are geometrically favourable and contribute cumulatively to crystal stability.

Further short contacts include the interaction between H2A and N1 (2.950 Å), as well as between H2A and C8 (3.052 Å), suggesting the presence of both C–H···N and C–H···C inter-

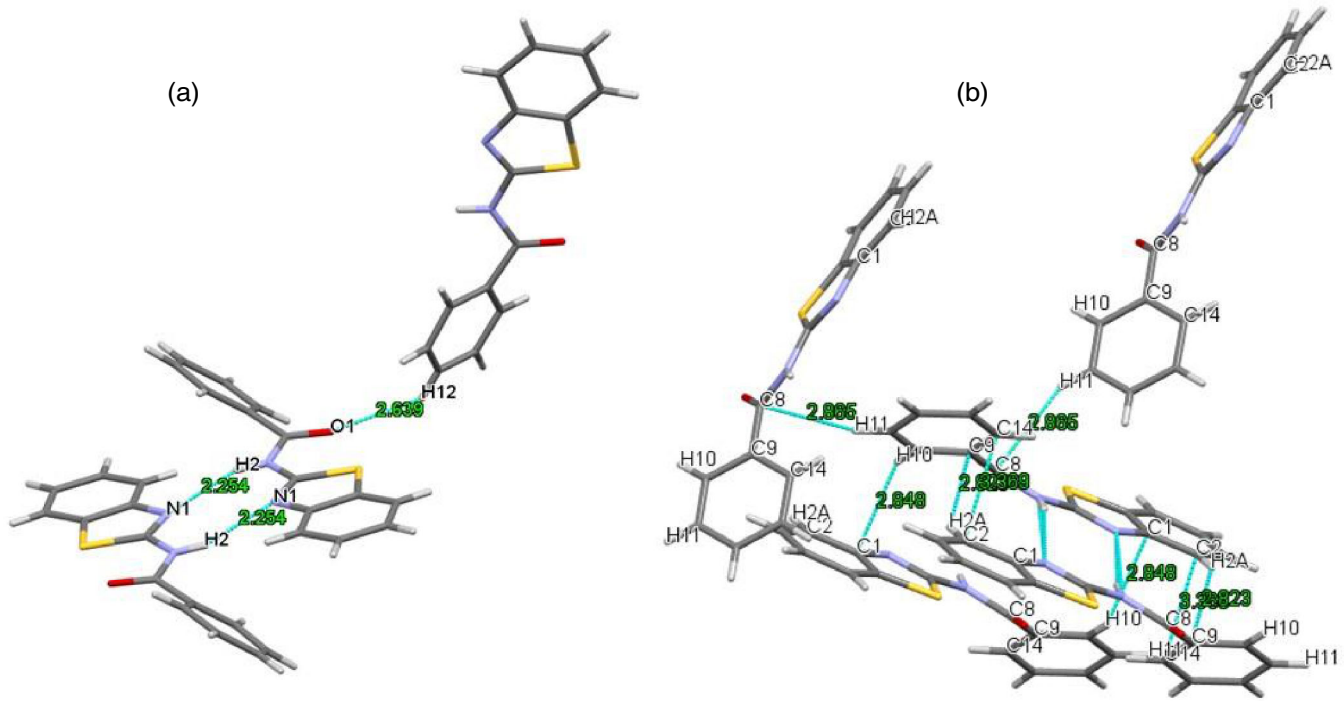

Fig. 2. Intermolecular interactions observed in the crystal structure of SIBO. (a) Depiction of hydrogen bonding interactions involving N–H···O and N–H···N contacts; (b) Illustration of other significant short contacts including C–H···π and π···π stacking interactions that contribute to the crystal packing

actions. Although C–H···C interactions are considered non-classical and weaker, they can play a critical role in crystal engineering, particularly in systems where more conventional hydrogen bond donors are limited. Overall, the combination of these short contacts mainly C–H···O, C–H···N and C–H···C interactions form an intricate network of weak intermolecular forces that guide molecular alignment and packing in the crystalline state of SIBO, thereby enhancing the overall structural cohesion. Collectively, these non-covalent interactions play a crucial role in governing the crystal packing and may influence the physicochemical properties of the compound in the solid state. The newly obtained crystal data aligns with previously reported structural parameters, confirming consistency in core molecular geometry, while also revealing new features that offer fresh insights into the intermolecular interactions [27].

Planarity and conformational analysis: To assess the degree of planarity and spatial arrangement of SIBO plane analysis was carried out using Mercury crystallographic software (Fig. 3). Molecule features a 2-aminobenzothiazole core connected *via* a carbonyl linkage (–C=O–) to a terminal phenyl ring. For planarity assessment, two mean planes were defined, the first encompassing the atoms of the aminobenzothiazole ring along with the attached carbonyl group and the second spanning the atoms of the terminal phenyl ring. The dihedral angle between these two planes was calculated to be 44.16º, indicating a moderate torsion between the two aromatic systems. This deviation from coplanarity can be attributed to the restricted rotation around the amide bond, which exhibits partial double-bond character as well as steric interactions between the adjacent rings. As a result, π-conjugation between the aminobenzothiazole and phenyl rings is interrupted, leading to localized electronic effects. However, this non-planar conformation may prove advantageous for biological interactions, as it allows the molecule to adopt a bent geometry suitable for fitting into non-planar or sterically hindered binding pockets. Moreover, the amide linkage itself may participate in hydrogen bonding, further contributing to potential interactions with target biomolecules. Overall, the observed torsion is a critical structural feature that may influence the bioactivity and binding behaviour of compound.

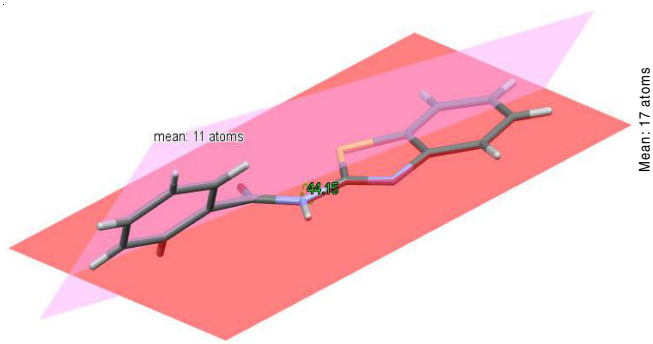

Fig. 3. Dihedral angle (44.18º) between the two aromatic ring planes in compound SIBO, showing a twisted molecular conformation

Structural agreement between DFT and XRD results: To evaluate the electronic behaviour and reactivity of the synthesized compound SIBO, DFT calculations were performed. The theoretical data obtained from DFT calculations and experimental data from single-crystal XRD (SC-XRD) analysis of the SIBO molecule were systematically compared. This comparison provides insight into the accuracy of the computational model by evaluating the agreement between the optimized geometry and the experimentally determined molecular structure in terms of bond lengths and bond angles (Tables 1 and 2).

TABLE-1
COMPARISON BETWEEN SELECTED BOND LENGTHS

Bond length	DFT	XRD
S1-C6	1.763	1.739(4)
N1-C1	1.387	1.398(5)
C7-S1	1.772	1.745(4)
N2-C7	1.384	1.385(5)
C8-N2	1.383	1.362(5)
O1-C8	1.226	1.220(6)
H4-C4	1.086	0.930
H2-N2	1.011	0.860

TABLE-2
COMPARISON BETWEEN SELECTED BOND ANGLES

Bond angle	DFT	XRD
S1-C6-C1	109.779	109.8(3)
C5-C6-S1	128.775	128.5(3)
N1-C1-C6	115.318	115.7(3)
C2-C1-N1	125.1	124.8(4)
C7-S1-C6	87.286	88.0
N2-C7-S1	122.373	122.0(3)
C8-N2-C7	126.06	124.1(3)
C9-C8-N2	116.157	115.4(3)
O1-C8-N2	121.225	121.9(4)
H2-N2-C8	120.407	117.9

The comparison between the DFT optimized structure and the XRD data for the SIBO compound reveals a high degree of consistency. Most bond lengths and angles obtained from theoretical calculations closely match the experimental values, with only slight deviations observed, primarily in hydrogen-involved bonds due to the limitations of XRD in accurately locating hydrogen atoms. This strong agreement highlights the accuracy of the DFT method in predicting molecular geometry and confirms the structural integrity of the model in representing the solid-state configuration of the compound.

FMO analysis: The energy levels and spatial distributions of the frontier molecular orbitals specifically the highest occupied molecular orbital (HOMO) and lowest unoccupied molecular orbital (LUMO) were analyzed to understand its potential reactivity, stability and possible electronic transitions (Fig. 4). For SIBO, the HOMO (orbital 66) is localized over the benzothiazole core, particularly on the sulfur and nitrogen atoms and also extends into the amide linkage. The LUMO (orbital 67), in contrast, is distributed mainly across the benzoyl phenyl ring and the amide substituent, indicating potential for $\pi \rightarrow \pi^*$ or $n \rightarrow \pi^*$ electronic transitions.

The HOMO–LUMO energy gap for SIBO is 0.159 a.u., equivalent to approximately 4.33 eV. indicates a moderate level of electronic stability alongside sufficient reactivity. This balance suggests that SIBO may be responsive to electron transfer pro-

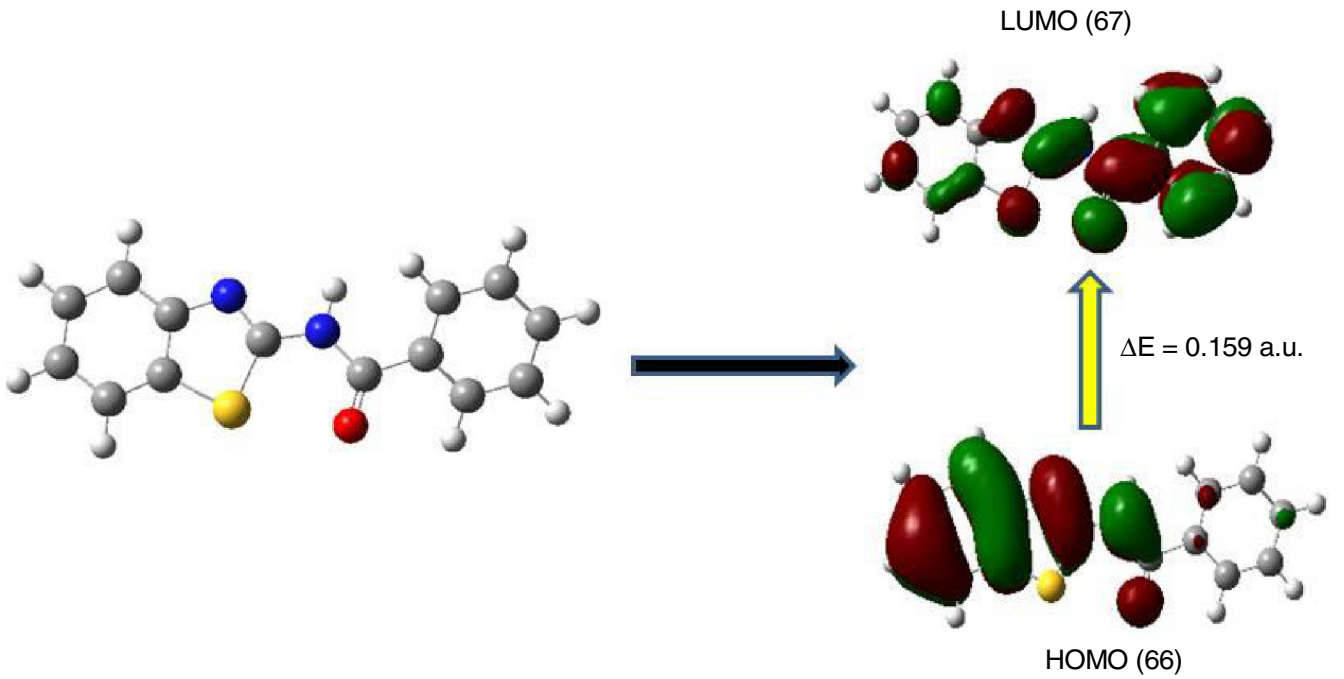

Fig. 4. Visualization of HOMO and LUMO orbitals in SIBO with a DFT derived energy gap

cesses and capable of interacting with biological macromolecules, which is advantageous for potential pharmacological or bioactive applications. Overall, SIBO exhibits extensive π-conjugation and favourable orbital overlap between the HOMO and LUMO.

Hirshfeld surface analysis: To investigate the molecular interaction landscape and crystal packing features of the synthesized compound SIBO, various Hirshfeld surface descriptors, namely d_i, d_e, fragment patch, shape index and curvedness, were computed (Fig. 5). The di and de surfaces for SIBO exhibited prominent red patches corresponding to short contacts such as N–H···O and C–H···π interactions. These features reflect the presence of significant hydrogen bonding and electrostatic interactions within the crystal structure. The fragment patch surface of SIBO revealed well-defined segmentation, indicating distinct molecular regions engaged in intermolecular interactions. The shape index map showed alternating red and blue triangular patches, characteristic of π···π stacking interactions between aromatic rings. This observation highlights the planar aromatic nature of SIBO and the crucial role of π-stacking in crystal stabilization. The curvedness surface revealed extended flat regions (blue-green zones), suggesting the presence of π-interactions and molecular co-planarity, while localized high-curvature zones indicated edge-to-face interactions or packing voids. The distribution and intensity of these interaction hotspots are influenced by the presence of amide and carbonyl functional groups in SIBO, shaping its unique intermolecular contact profile. These surface analyses complement the fingerprint plots and provide a 3D visualization of how molecular geometry and functional groups govern the solid-state packing and intermolecular interaction networks in SIBO.

To gain a more direct and quantitative visualization of intermolecular interactions, especially hydrogen bonding and close contacts, the d_{norm} surface of SIBO, mapped over the range 0.2654 to 1.2667 a.u., distinctly highlights interaction hotspots as intense red regions, which correspond to close intermolecular contacts. Notably, two significant red spots labelled 1 and 2 (Fig. 6) indicate the presence of strong hydrogen bonding interactions, likely involving classical donors such as NH groups. Complementary to this surface analysis, the 2D fingerprint plots offer a quantitative breakdown of the various intermolecular contacts contributing to the crystal packing. The H···H interactions, accounting for 31.2% of total contacts, appear as a broad central region and represent prevalent van der Waals forces that contribute to general lattice stabilization. The C···H/H···C contacts contribute 34.3% and are visualized as symmetrical wing-like features, typically associated with weak C–H···π interactions that aid molecular cohesion. The O···H/H···O interactions, contributing 9.6%, form sharp spikes, indicative of strong, directional hydrogen bonding, likely involving hydroxyl or amide functionalities. The N···H/H···N contacts, with an 8.2% contribution, also exhibit sharp spikes in the plot, supporting the involvement of amine NH groups in hydrogen bonding with nitrogen acceptors. Moreover, the S···H/H···S interactions contributing 8.4%, manifest as moderately sharp spikes. The total fingerprint plot reflects a well-defined distribution of contact types, confirming the complexity of the intermolecular network. The electrostatic potential mapped onto the surface further supports these findings, with electron-rich (red) and electron-poor (blue) regions corresponding to likely hydrogen bond acceptors and donors, respectively. In summary, although dispersive H···H and C···H interactions dominate the surface, the sharp spikes corresponding to O–H···O and N–H···N interactions underscore the crucial role of strong, directional hydrogen bonding in stabilizing the crystal structure of SIBO. The additional contribution from sulfur involves interactions that further enhance the complexity and robustness of molecular assembly in the solid state.

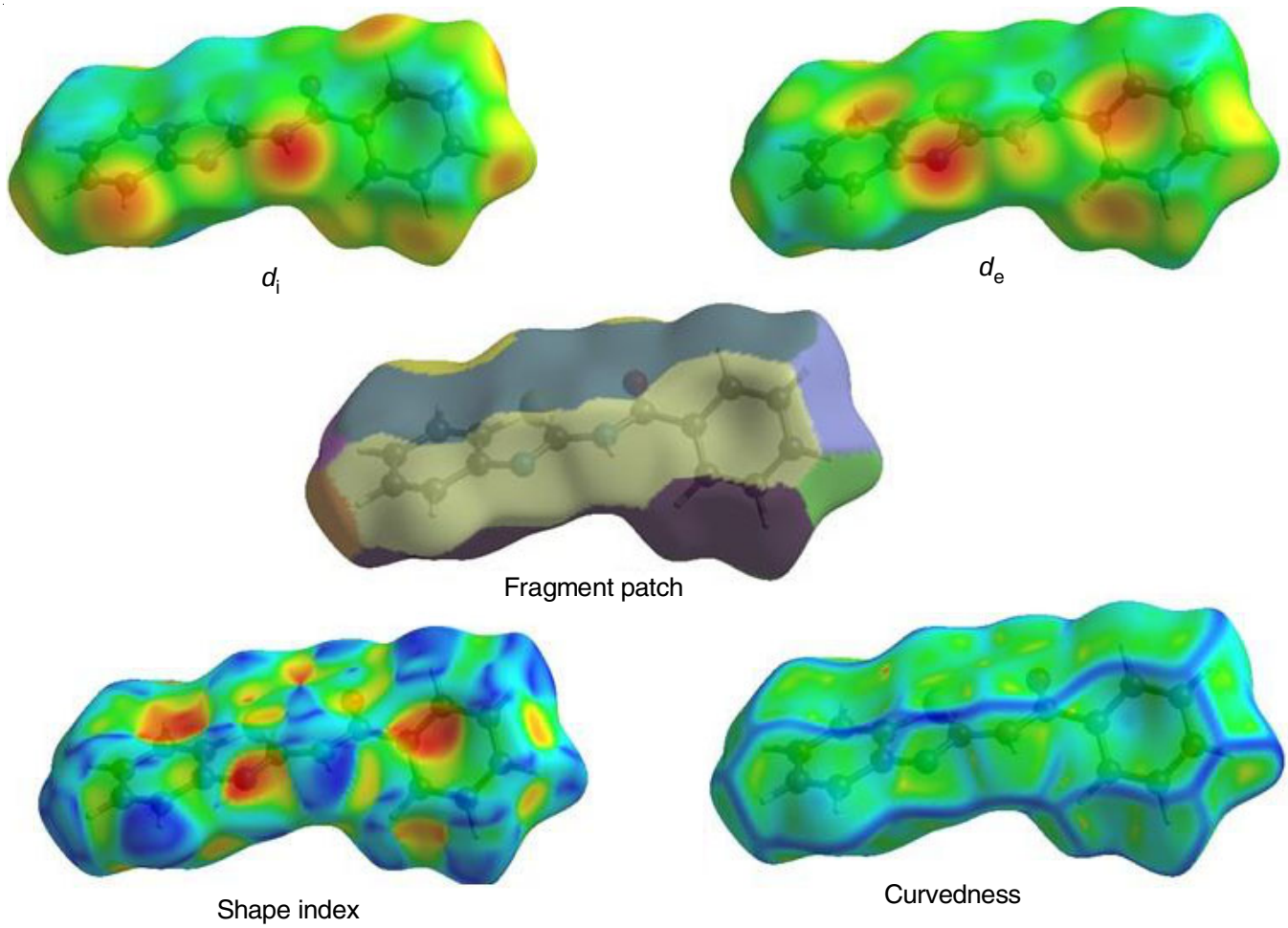

Fig. 5. Surface property visualizations of compound SIBO depicting molecular descriptors relevant to binding interactions

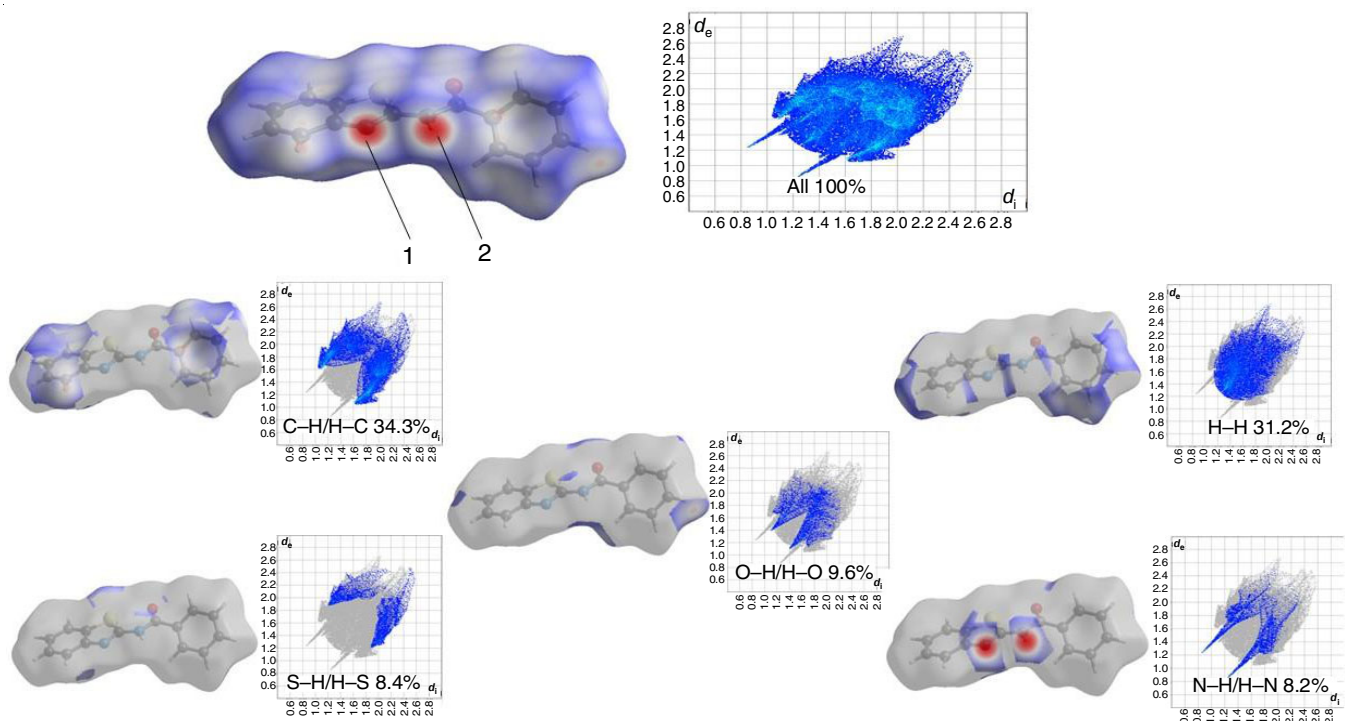

Fig. 6. Hirshfeld surface analysis of SIBO, the d_{norm} surface highlights key intermolecular contacts (1 and 2). 2D fingerprint plots show major interactions contributing to crystal packing

Anticancer activity: The synthesized compound SIBO was evaluated for its *in vitro* anticancer activity using the MDA-MB-231 (triple-negative) and MCF-7 (estrogen receptor-positive) breast cancer cell lines, employing the sulforhodamine B (SRB) assay, with adriamycin (ADR) serving as the standard control (Fig. 7) [28]. In MDA-MB-231 cell line, SIBO demonstrated significant cytostatic activity, with 52.0% inhibition at 10 µg/mL, 32.9% inhibition at 40 µg/mL and 28.2% inhibition at 80 µg/mL. These results indicate a dose-dependent reduction in cell growth, suggesting that SIBO holds potential as a lead compound for further optimization. For comparison, ADR, a well-established chemotherapeutic agent, produced strong cytotoxic effects, with growth inhibition of 82.9% at 40 µg/mL and 100% inhibition at 80 µg/mL. While ADR is significantly more potent in its activity, the moderate effect of SIBO is promising, as it suggests that these compounds could offer a less toxic alternative with less aggressive side effects, which could be important in the development of novel anticancer drugs. When tested against the MCF-7 cell line, SIBO again showed moderate activity, with 14.3% inhibition at 10 µg/mL, 13.2% inhibition at 40 µg/mL and 21.7% inhibition at 80 µg/mL. This was slightly less potent than in the MDA-MB-231 line, but still indicates that SIBO could be effective across different breast cancer subtypes. While SIBO does not reach the extreme potency of ADR, the data indicate that this compound shows promising anticancer activity. This compound demonstrates dose-dependent inhibition and its moderate activity suggests it may offer safer alternatives with less toxicity than traditional chemotherapeutics. The findings support further optimization of these compounds for use in cancer therapy, focusing on improving their selectivity and targeting mechanisms. This provides a strong foundation for their future development as anticancer agents. The observed anticancer activity of our synthesized molecule aligns with that of previously reported compounds of a similar structural class, demonstrating comparable cytotoxicity against breast cancer cells [29,30].

Conclusion

2-Aminobenzothiazole derivative (SIBO) was efficiently synthesized *via* copper(I) bromide-catalyzed tandem reaction between benzoyl isothiocyanate and 2-haloaniline. Its structure was confirmed by single-crystal X-ray diffraction, revealing a monoclinic system stabilized by hydrogen bonding and π–π stacking. Density functional theory (DFT) calculations supported the experimental geometry and highlighted a moderate HOMO–LUMO energy gap, suggesting potential biological activity. Hirshfeld surface analysis further clarified the nature of intermolecular interactions, affirming structural stability. Biological evaluation of SIBO through *in vitro* anticancer assays revealed dose-dependent cytostatic activity, particularly against the MDA-MB-231 (triple-negative) breast cancer cell line, with up to 52.0% inhibition at 10 µg/mL. While standard adriamycin exhibited greater potency, the moderate activity of SIBO across both MDA-MB-231 and MCF-7 lines suggests a potential for lower toxicity and selectivity toward diverse cancer subtypes. These findings, supported by structure-activity considerations, position SIBO as a promising scaffold for further derivatization and lead optimization in anticancer drug development.

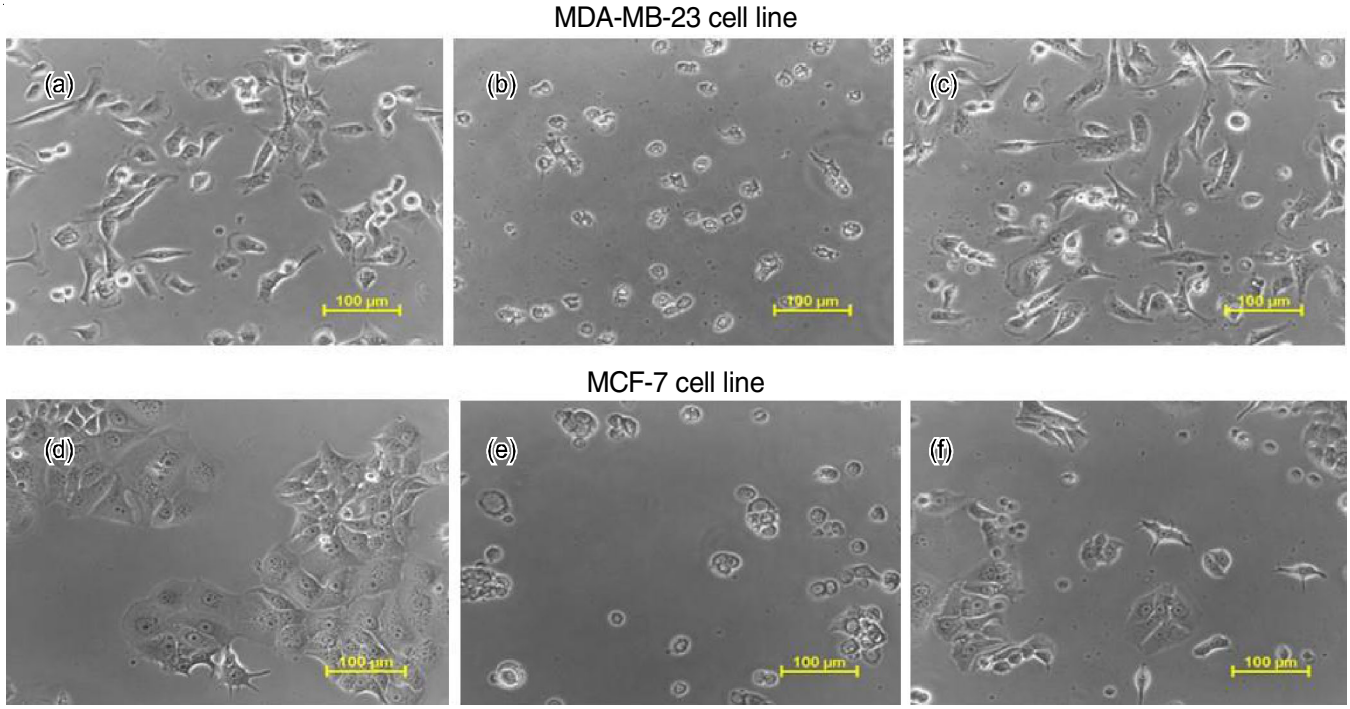

Fig. 7. Microscopic images showing the morphological changes in MDA-MB-231 (top row: a to c) and MCF-7 (bottom row: d to f) human breast cancer cell lines after treatment with compound SIBO. Images (a) and (d) represent untreated control cells exhibiting normal morphology, while (b) and (e) show cells treated with a standard drug ADR (positive control), demonstrating noticeable cytotoxic effects. Images (c) and (f) correspond to cells treated with compound SIBO, revealing altered cellular morphology, decreased cell density and characteristic signs of apoptosis. All images were captured at a scale of 100 µm using a phase-contrast microscope

ACKNOWLEDGEMENTS

The authors gratefully acknowledge the Advanced Centre for Treatment, Research and Education in Cancer (ACTREC), Tata Memorial Centre, for providing the necessary facilities and support for this research work.

CONFLICT OF INTEREST

The authors declare that there is no conflict of interests regarding the publication of this article.

REFERENCES

1. S.E.H. Etaiw, D.M. Abd El-Aziz, E.H. Abd El-Zaher and E.A. Ali, *Spectrochim. Acta A Mol. Biomol. Spectrosc.*, **79**, 1331 (2011); https://doi.org/10.1016/j.saa.2011.04.064
2. J. Joseph and G. Boomadevi Janaki, *J. Mol. Struct.*, **1063**, 160 (2014); https://doi.org/10.1016/j.molstruc.2014.01.028
3. Z. Gul, N.U. Din, E. Khan, F. Ullah and M. Nawaz Tahir, *J. Mol. Struct.*, **1199**, 126956 (2020); https://doi.org/10.1016/j.molstruc.2019.126956
4. S.S. Awaad, M.O. Sarhan, W.R. Mahmoud, T. Nasr, R.F. George and H.H. Georgey, *J. Mol. Struct.*, **1291**, 136042 (2023); https://doi.org/10.1016/j.molstruc.2023.136042
5. T.L. Dadmal, S.D. Katre, M.C. Mandewale and R.M. Kumbhare, *New J. Chem.*, **42**, 776 (2018); https://doi.org/10.1039/C7NJ03776G
6. K.P. Yadav, M.A. Rahman, S. Nishad, S.K. Maurya, M. Anas and M. Mujahid, *Intell. Pharm.*, **1**, 122 (2023); https://doi.org/10.1016/j.ipha.2023.06.001
7. L.V. Zhilitskaya, B.A. Shainyan and N.O. Yarosh, *Molecules*, **26**, 2190 (2021); https://doi.org/10.3390/molecules26082190
8. M. Neetha, S.B. Umabharathi and G. Anilkumar, *Catal. Lett.*, **155**, 15 (2025); https://doi.org/10.1007/s10562-024-04835-3
9. R. Javahershenas, J. Han, M. Kazemi and P.J. Jervis, *ChemistryOpen*, **13**, e202400185 (2024); https://doi.org/10.1002/open.202400185
10. Q. Ding, B. Cao, X. Liu, Z. Zong and Y.-Y. Peng, *Green Chem.*, **12**, 1607 (2010); https://doi.org/10.1039/c0gc00123f
11. Q. Ding, X. He and J. Wu, *J. Comb. Chem.*, **11**, 587 (2009); https://doi.org/10.1021/cc900027c
12. K. Yadav, J. Dhankhar and P. Kundu, *Curr. Res. Nutr. Food Sci.*, **10**, 476 (2022); https://doi.org/10.12944/CRNFSJ.10.2.6
13. T. Qadir, A. Amin, A. Salhotra, P.K. Sharma, I. Jeelani and H. Abe, *Curr. Org. Chem.*, **26**, 189 (2022); https://doi.org/10.2174/1385272826666211229144446
14. R. Dass and M.A. Peterson, *Tetrahedron Lett.*, **83**, 153388 (2021); https://doi.org/10.1016/j.tetlet.2021.153388
15. N.M. Anjalin, N. Kanagathara and A.R. Baby Suganthi, *Mater. Today Proc.*, **33**, 4751 (2020); https://doi.org/10.1016/j.matpr.2020.08.358
16. L. Romeo, R. Iori, P. Rollin, P. Bramanti and E. Mazzon, *Molecules*, **23**, 624 (2018); https://doi.org/10.3390/molecules23030624
17. C.C. Hoch, M. Shoykhet, T. Weiser, L. Griesbaum, J. Petry, K. Hachani, G. Multhoff, A. Bashiri Dezfouli and B. Wollenberg, *Pharmacol. Res.*, **201**, 107107 (2024); https://doi.org/10.1016/j.phrs.2024.107107
18. K.K. Brown and M.B. Hampton, *Biochim. Biophys. Acta, Gen.*, **1810**, 888 (2011); https://doi.org/10.1016/j.bbagen.2011.06.004
19. P.M. Wanjari, S.N. Mokale, A.V. Bharati and V.N. Ingle, *Med. Chem. Res.*, **30**, 655 (2021); https://doi.org/10.1007/s00044-020-02671-9
20. Z.F. AI-Janahi and M.H. Said, *Pharm. Med. Sci.*, **2**, (2025); https://doi.org/10.62846/3006-5909.1018
21. G.M. Sheldrick, *Acta Crystallogr. C Struct. Chem.*, **71**, 3 (2015); https://doi.org/10.1107/S2053229614024218
22. L.J. Farrugia, *J. Appl. Cryst.*, **30**, 565 (1997); https://doi.org/10.1107/S0021889897003117
23. C.F. Macrae, I. Sovago, S.J. Cottrell, P.T.A. Galek, P. McCabe, E. Pidcock, M. Platings, G.P. Shields, J.S. Stevens, M. Towler and P.A. Wood, *J. Appl. Cryst.*, **53**, 226 (2020); https://doi.org/10.1107/S1600576719014092
24. M.J. Frisch, G.W. Trucks, H.B. Schlegel, G.E. Scuseria, M.A. Robb, J.R. Cheeseman, G. Scalmani, V. Barone, B. Mennucci, G.A. Petersson, H. Nakatsuji, M. Caricato, X. Li, H.P. Hratchian, A.F. Izmaylov, J. Bloino, G. Zheng, J.L. Sonnenberg, M. Hada, M. Ehara, K. Toyota, R. Fukuda, J. Hasegawa, M. Ishida, T. Nakajima, Y. Honda, O. Kitao, H. Nakai, T. Vreven, J.A. Montgomery, Jr., J.E. Peralta, F. Ogliaro, M. Bearpark, J.J. Heyd, E. Brothers, K.N. Kudin, V.N. Staroverov, R. Kobayashi, J. Normand, K. Raghavachari, A. Rendell, J.C. Burant, S.S. Iyengar, J. Tomasi, M. Cossi, N. Rega, J.M. Millam, M. Klene, J.E. Knox, J.B. Cross, V. Bakken, C. Adamo, J. Jaramillo, R. Gomperts, R.E. Stratmann, O. Yazyev, A.J. Austin, R. Cammi, C. Pomelli, J.W. Ochterski, R.L. Martin, K. Morokuma, V.G. Zakrzewski, G.A. Voth, P. Salvador, S. Dapprich, J.J. Dannenberg, A.D. Daniels, Ö. Farkas, J.B. Foresman, J.V. Ortiz, J. Cioslowski and D.J. Fox, Gaussian 09, Revision D.01, Gaussian, Inc., Wallingford CT (2009).
25. R. Dennington, T.A. Keith and J.M. Millam, GaussView, version 6.0. vol. 16, Semichem Inc., Shawnee Mission (2016).
26. M.A. Spackman and D. Jayatilaka, *CrystEngComm*, **11**, 19 (2009); https://doi.org/10.1039/B818330A
27. J. Angulo-Cornejo, M. Lino-Pacheco, R. Richter, L. Hennig, K.-H. Hallmeier and L. Beyer, *Inorg. Chim. Acta*, **305**, 38 (2000); https://doi.org/10.1016/S0020-1693(00)00109-2
28. V. Vichai and K. Kirtikara, *Nat. Protoc.*, **1**, 1112 (2006); https://doi.org/10.1038/nprot.2006.179
29. F. Corbo, A. Carocci, D. Armenise, N. De Laurentis, A. Laghezza, F. Loiodice, P. Ancona, M. Muraglia, V. Pagliarulo, C. Franchini and A. Catalano, *J. Chem.*, **2016**, 1 (2016); https://doi.org/10.1155/2016/4267564
30. A. Irfan, F. Batool, S.A.Z. Naqvi, A. Islam, S.M. Osman, A. Nocentini, S.A. Alissa and C.T. Supuran, *J. Enzyme Inhib. Med. Chem.*, **35**, 265 (2020); https://doi.org/10.1080/14756366.2019.1698036